NANO LETTERS

2007
Vol. 7, No. 12
3849−3853

Nanodisk Codes

Lidong Qin,† Matthew J. Banholzer,† Jill E. Millstone,† and Chad A. Mirkin*

Department of Chemistry and International Institute for Nanotechnology, Northwestern University, 2145 Sheridan Road, Evanston, Illinois 60208-3113

Received October 9, 2007; Revised Manuscript Received November 6, 2007

ABSTRACT

We report a new encoding system based upon dispersible arrays of nanodisks prepared by on-wire lithography and functionalized with Raman active chromophores. These nanodisk arrays are encoded both physically (in a "barcode" pattern) and spectroscopically (Raman) along the array. These structures can be used in covert encoding strategies because of their small size or as biological labels with readout by scanning confocal Raman spectroscopy. As proof-of-concept, we demonstrate their utility in DNA detection in a multiplexed format at target concentrations as low as 100 fM.

Encoded materials are used for many applications, including cryptography, computation, brand protection, covert tracking of material goods and personnel, and labeling in biological and chemical diagnostics.[1−5] Often, nanostructures are appealing materials for encoding applications because they can be dispersed or hidden in a variety of media due to their small size, and their chemical and physical properties can be rationally designed in a variety of ways.[6−9] In addition, certain types of nano- and micromaterials are beginning to find application as probes in sensitive and selective molecular diagnostic systems.[5,6,9] These materials include nanoparticles labeled with Raman chromophores,[10] striped nanorods,[11−13] and several types of beads modified with fluorophores[5,14−17] such as organic dyes and inorganic quantum dots.[14−17] Striped nanorods are a particularly interesting class of materials because they are dispersible entities, allow for massive encoding based upon the length and location of individual chemical blocks within the structures, and can be functionalized using conventional surface chemistries.[11] These nanostructures are typically identified by reflectivity or fluorescence. However, the high degree of overlap between common fluorescent labels, the quenching properties of the metal blocks that comprise the structures, and the difficulty in resolving differences in metal reflectivity represent limitations for these systems.[11,12] Herein, we report a new encoding system based upon dispersible arrays of nanodisks prepared by on-wire lithography (OWL) and functionalized with Raman active chromophores. These nanodisk arrays are encoded both physically (in a "barcode" pattern) and spectroscopically (Raman) along the array. These structures can be used in covert encoding strategies because of their small size or as biological labels with readout by scanning Raman spectroscopy.

Recently, we reported a process called OWL that allows one to tailor the physical and chemical structure of nanorods to generate a class of nanostructures not accessible by conventional synthetic or lithographic processes.[18,19] Specifically, one can make dispersible, segmented nanorod structures of fixed diameters with gap separations and disk features well-defined along the length of the nanostructure. Gaps between metal sections can be fabricated with dimensions from 2 nm to many μm. This high degree of tailorability has allowed us to probe the relationship between feature size, gap size, and Raman-enhancing properties in such a way that we can identify the maximum enhancing structure for a class of disk materials fabricated by OWL.[19] By site isolating disk pairs along the long axis of a nanorod, we can use confocal Raman microscopy (CRM) to independently address each disk pair. On the basis of the observation that one can create Raman hot spots at specific locations along the long axis of the rod, we hypothesized that one could use disk pair structures that exhibit large enhancements in a novel encoding scheme. Once functionalized with the appropriate chromophores, these nanodisk codes (NDCs) can be identified easily by Raman spectroscopy and take advantage of the well-known surface-enhanced Raman scattering (SERS) phenomenon.[10,16,19−23] In principle, one can generate a myriad of nanodisk codes simply by varying the number and location of the pairs as well as the type and number of chromophores used as spectroscopic labeling agents. This multilevel approach to encoding nanostructures avoids some of the limitations of striped barcodes by transitioning weaknesses such as fluorescence quenching into advantages in the context of the Raman format. Herein, we report the synthesis, functionalization, and use of NDCs in the context of both physical and nucleic acid labeling.

In a typical experiment, 360 nm diameter Au−Ni nanorods are synthesized by template-directed electrochemical syn-

* Corresponding author. E-mail address: chadnano@northwestern.edu.
† These authors contributed equally to this work.

10.1021/nl072606s CCC: $37.00
Published on Web 11/28/2007

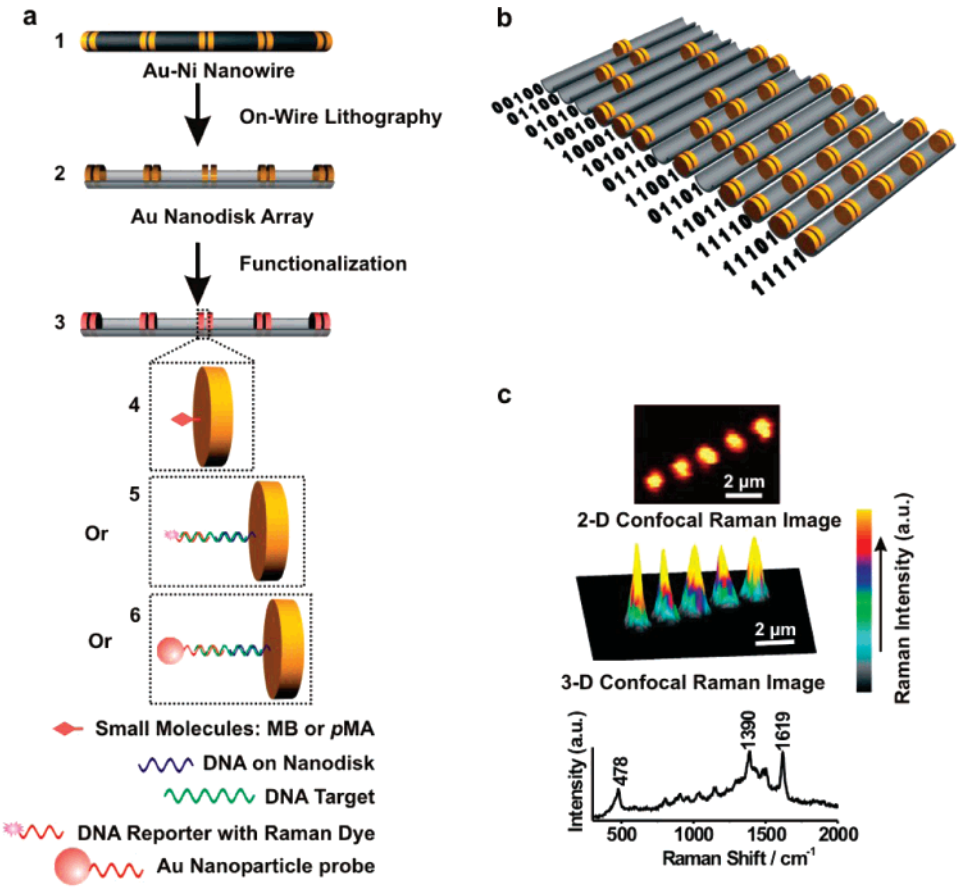

Figure 1. Scheme of the NDC method. (a) Synthesis and functionalization. (b) Thirteen possible 5-disk-pair NDCs with corresponding binary codes. (c) 2D (top) and 3D (middle) scanning Raman microscopy images of a 11111 NDC. Representative Raman spectrum of MB (bottom) taken from the center of the hot spot generated in the middle disk pair shown in the Raman maps above.

thesis[24−26] and then converted to disk arrays using OWL methodology (Figure 1A, Supporting Information Figure S1).[18] This approach has allowed us to design SERS-optimized Au nanodisk arrays consisting of spatially separated disk pairs and to assign a binary coding scheme to these disk pair arrays, where the presence of a disk pair is represented by the number one, and the absence of a disk pair is represented by a zero. For example, if the middle (third) disk pair in a five pair array is intentionally omitted by depositing Ni in place of an Au disk pair, a code of 11011 is generated. Alternatively, a 10101 barcode is prepared by replacing the second and the fourth Au disk pairs with Ni during the deposition process. With 5 pairs of disks, this encoding scheme, based solely on the location and number of disk pairs, yields 13 distinct NDCs when redundant sequences are eliminated (Figure 1B). The number of unique coding structures that are available increases exponentially simply by generating longer arrays with more disk pairs (e.g., 25 disk pairs $= 2.7 \times 10^6$ unique codes; see Supporting Information for growth calculation and Figure S2).

As proof-of-concept, we have fabricated three representative NDCs: 11111, 11011, and 10101 codes, (field emission scanning electron microscopy (FE-SEM), Supporting Information Figure S1A−C). The Au NDCs **2** are functionalized with a Raman label to yield Raman-active NDCs **3** (Figure 1A). For the purposes of this study, we have used methylene blue (MB) and para-mercaptoaniline (pMA), two commonly used dyes available from a wide library of Raman chromophores.[27,28] These serve as NDC labels **4** that enable either redundant or complementary detection methods. In this work, these Raman-active molecules are immobilized on the surface of the nanodisk code, where each spot in this array exhibits a SERS enhancement factor of 4.6×10^8 (see Supporting Information for details of functionalization and calculation).[19] Note that we have made arrays as long as 12 μm thus far, which can support as many as 10 independently addressable disk pairs and 287 disk codes based upon physical encoding alone (see Supporting Information Figure S3).

The Raman-active NDCs **4** were characterized by CRM by integrating the entire spectral intensity from 139 to 2789 cm^{-1}. In this mode, the disk pair features appear as fully resolved bright spots against a dark, smooth background in both the two- (2D) and three-dimensional (3D) images (Figure 1C, top, middle). Additionally, a full Raman spectrum is recorded at each pixel of the image and provides Raman fingerprint information to accurately assign the labeled NDC (Figure 1C, bottom).

It is important to note that this approach does not work with the conventional striped metal barcodes, because the disk pairs and optimized gaps are required to achieve high levels of enhanced spectroscopic responses (the optimized architectural parameters for these disk pairs has been

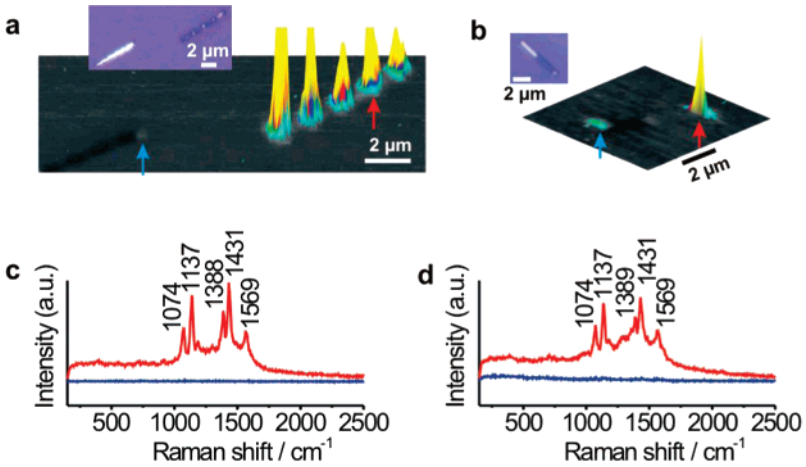

Figure 2. Comparison of Raman signals in NDCs and conventional striped metal barcodes. (a) Optical (inset) and scanning Raman 3D images of a Au−Ni nanorod (left), a 11111 NDC (right) and (b) an Au nanorod−disk pair array. (c,d) Raman spectra taken at discrete locations designated by red and blue arrows in (a,b) respectively.

determined previously).[19] To illustrate the importance of the OWL-generated architecture, we prepared an aqueous solution of pre-etched wires (analogous to striped barcodes) and NDCs (made from these pre-etched wires) and simultaneously labeled them with pMA (see Supporting Information). Both structures were characterized by dark field microscopy and scanning Raman spectroscopy (Figure 2A,C). Note that each of the five disk pairs of the 11111 NDC exhibits a strong Raman response (Figure 2A, (right) and C (red)) while the unetched structure exhibits almost no signal intensity (Figure 2A (left) and C (blue)). Indeed, the signal intensity of the spectra resulting from the Au disk codes is 142 000 charge-coupled device (CCD) counts higher than the spectra corresponding to the striped wires (calculated by numerically integrating the spectra associated with the locations at the red and blue arrows in Figure 2A). The ratio of signal intensity between the NDC and unetched wires is approximately 143:1 (normalized for background). To determine if this signal difference was due to differences in surface area, we designed a nanorod structure that contained both a single disk pair and a long Au nanorod segment, where the surface area ratio between the nanorod section and the disk pair is 9:2 (FE-SEM image, Supporting Information Figure S1E). After functionalizing this structure with pMA, we see that the signal intensity from the disk pair is 92 times higher (∼91 000 CCD counts) than the nanorod, despite the much larger surface area and number of chromophores immobilized on the conventional nanorod segment (Figure 2B,D).

This binary physical encoding coupled with the high-sensitivity Raman readout makes these disk codes attractive as labels in biological tagging schemes. Accordingly, as proof-of-concept we have investigated the use of NDCs in a three-strand sandwich scheme (Figure 3A). In these experiments, thiol-modified single-stranded DNA (ssDNA) molecules were attached to the NDC surfaces according to previously published protocols used for gold spherical nanoparticles.[9] These oligonucleotides contained a sequence complementary to one-half of a target ssDNA sequence. The remaining half of the target sequence is complementary to a reporter strand that contains a Raman-active probe. Because the disk pairs generate a SERS-enhancement factor of over 8 orders of magnitude (see Supporting Information), even a small number of binding events can be detected by CRM (Figure 1A, panel 5). In principle, it has an inherent multiplexing capability due to the "barcode" nature of the structures.

To confirm and demonstrate this capability, we employed a three-strand DNA detection system as described above wherein 11011 nanodisk codes are functionalized with an oligonucleotide sequence (called "NDC_{11011}") that we designed to be complementary to a section of a DNA target ($target_{11011}$). The complement to the second half of this target sequence contained a Cy5 reporter molecule ($reporter_{11011}$) (Figure 3A). In a different solution, we functionalized 10101-encoded NDCs with a second sequence (NDC_{10101}), which is complementary to one-half of a second DNA target ($target_{10101}$); the complement to the second half of this target sequence contained a TAMRA reporter molecule ($reporter_{10101}$) (Figure 3A). We then mixed the functionalized 11011 and 10101 NDCs, both target sequences and both reporter strands in the same solution, and allowed the oligonucleotides to hybridize at 37 °C. When both $target_{11011}$ and $target_{10101}$ are present, positive images are obtained for both 11011 and 10101 disk codes (Figure 3B). Because the Raman image map contains full Raman spectral information for both Cy5 and TAMRA embedded in every pixel, we were able to specifically monitor the Raman band ranging from 525.2 to 592.4 cm^{-1} from Cy5 and apply a filter to the signal output (blue bar, Figure 3E). By doing so, we have demonstrated that only $target_{11011}$ and $reporter_{11011}$ DNA are present on 11011 disk codes (Figure 3C). Likewise, we have monitored the Raman band ranging from 1630.0 to 1679.0 cm^{-1} from TAMRA, applied a similar filter (red bar, Figure 3E), and demonstrated that only $target_{10101}$ and $reporter_{10101}$ were present on 10101 disk codes (Figure 3D). It is important to note that the multiplexing ability of this system is a result of the binary coding architecture and not the different Raman dyes. In this case, two Raman dyes are used simply to illustrate the specificity of the system.

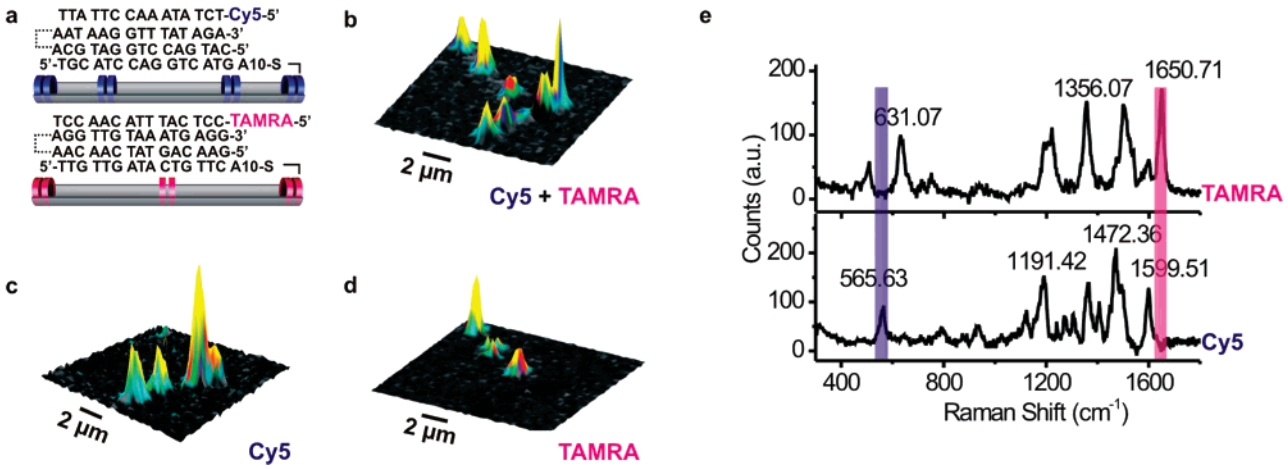

Figure 3. Multiplexing with NDCs. (a) Scheme of 11011 and 10101 NDC nanostructures showing DNA sequences of target, reporter, and NDC strands. (b) Full-spectrum 3D scanning Raman image of 11011 and 10101 disk codes functionalized with different single-stranded DNA sequences. (c) Filtered Raman image of (b) where the transmitted frequencies are indicated by the blue bar in (e), corresponding to a unique Raman band from the Cy5 reporter (525.2−592.4 cm^{-1}). (d) Filtered Raman image of (b) where the transmitted frequencies are indicated by the red bar in (a), corresponding to a unique Raman peak from the TAMRA reporter (1630.0−1679.0 cm^{-1}). (e) Raman spectra of Cy5 and TAMRA from reporter DNA sequences immobilized on NDC after DNA hybridization. N.B. (c,d) are taken with only a fraction of the total Raman signal being collected; the three images in (b−d) do not have the same *z*-scale and have been normalized for a straightforward comparison.

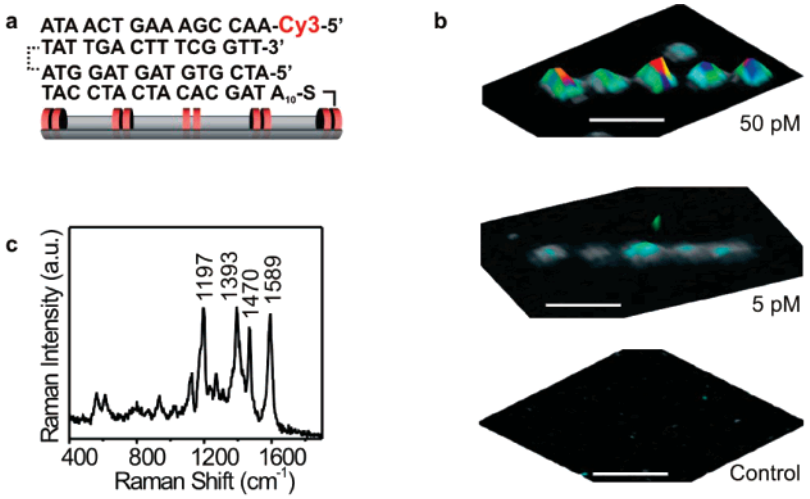

Figure 4. Three-strand sandwich DNA-labeling based on NDC and Raman probe. (a) Schematic representation of three-strand DNA system, including DNA sequences used in these experiments. (b) 3D scanning Raman images of DNA detection results at target concentrations of 50 pM, 5 pM, and control with no target (top to bottom, respectively). All three images are graphed with the same *z*-scale. The control experiment (with only reporter and NDC strands, and no target) does not give any readable response. (c) A representative Raman spectrum taken from 3D spectra in (b).

Using the NDCs in a sandwich format, we have detected target DNA at concentrations as low as 5 pM (Figure 4A). A control experiment containing the same amount of reporter sequences and NDCs, but without target DNA, shows no discernible Raman signal (Figure 4B). Each NDC can be readout within a time scale ranging from seconds to minutes, depending on the desired application (Supporting Information Figure S4). The limit of detection (LOD) is reasonably impressive, considering the assay has not been coupled with a secondary amplification scheme. Even at these low concentrations, the Raman lines (and thus the "fingerprint" character of the spectrum) are still readily observable (Figure 4C).

Additional sensitivity can be gained if one immobilizes reporter DNA strands on Au nanoparticles (NP) (diameter = 13 nm ± 5%). Using Raman-dye modified AuNPs has the potential to generate a 100-fold increase in signal intensity due to ~100 additional labeled strands being brought into the Raman hotspot per AuNP binding event. The nanoparticle also quenches the fluorescence of the Raman dye, which has been shown to interfere with Raman scattering. Using the NP-target-NDC sandwich assay **6** (Figure 1A), an LOD of 100 fM is achievable (Supporting Information Figures S5 and S6). A control experiment where NPs and NDCs are mixed without the presence of a target sequence shows no discernible response, and SEM of the NDCs after mixing confirms that no significant NP binding to the NDCs occurs.

In conclusion, we have developed a novel and potentially powerful encoding system based upon dispersible arrays of

nanodisks that are capable of high-sensitivity, multimodal reporting for both chemical and physical covert labeling as well as biomolecule detection. The NDCs are a versatile platform that can be easily tailored using a variety of parameters including chemical label type, disk pair number, and interdisk pair spacing. These NDCs have the inherent ability to employ labeling chromophores and physical architecture in redundant (where the dye label reporter serves to confirm the binary encoding data), collective (where both the label and the architecture give complementary encoding information), or independent methodologies (where only the label or binary structure is used). This flexibility can be expanded further by synthesizing NDCs with disk pairs of different metal compositions within the same array structure and functionalizing the different metals with distinct chemical moieties. This additional functionality will enable even more complex encoding structures, where information is stored within the physical architecture, and chemical labeling of a single disk array. The use of Raman spectroscopy and the narrow vibrational line signatures of the corresponding dyes (as opposed to the broad emission bands associated with fluorophores) allows one to consider a much larger library of dyes for multiplexing purposes. Finally, although the experiments reported herein are carried out using large, relatively costly instruments, with handheld conventional Raman spectrophotometers in the marketplace and portable scanning Raman instruments demonstrated in the lab,[29] mobile detection and encoding schemes based on the NDC system are possible.

Acknowledgment. C.A.M. acknowledges the U.S. Air Force Office of Scientific Research (AFSOR), Defense Advanced Research Projects Agency (DARPA), and the National Science Foundation (NSF) for support of this research. C.A.M is also grateful for an NIH Director's Pioneer Award. J.E.M. is grateful to Northwestern University for a Presidential Fellowship. The authors are grateful to Matthew G. Reuter for help on calculating NDC combinatorics.

Supporting Information Available: Detailed methods and materials; assignment of Raman Bands; DNA loading on Au disk surface; calculation of potential NDC structures; calculation of NDC enhancement factor; SEM images of nanorods; and additional 3D Raman scans. This material is available free of charge via the Internet at http://pubs.acs.org.

References

(1) Gershon, D. *Nature* **2002**, *416*, 885−891.
(2) Pregibon, D. C.; Toner, M.; Doyle, P. S. *Science* **2007**, *315*, 1393−1396.
(3) Nolan, J. P.; Sklar, L. A. *Trends Biotechnol.* **2002**, *20*, 9−12.
(4) Gunderson, K. L.; Kruglyak, S.; Graige, M. S.; Garcia, F.; Kermani, B. G.; Zhao, C.; Che, D.; Dickinson, T.; Wickham, E.; Bierle, J.; Doucet, D.; Milewski, M.; Yang, R.; Siegmund, C.; Haas, J.; Zhou, L.; Oliphant, A.; Fan, J.-B.; Barnard, S.; Chee, M. S. *Genome Res.* **2007**, *14*, 870−877.
(5) Wilson, R.; Cossins, A. R.; Spiller, D. G. *Angew. Chem., Int. Ed.* **2006**, *45*, 6104−6117.
(6) Nam, J.-M.; Thaxton, C. S.; Mirkin, C. A. *Science* **2003**, *301*, 1884−1886.
(7) Alivisatos, A. P. *Nat. Biotechnol.* **2004**, *22*, 47−52.
(8) Zheng, X.; Young, M. A.; Lyandres, O.; Van Duyne, R. P. *J. Am. Chem. Soc.* **2005**, *127* (12), 4484−4489.
(9) Rosi, N. L.; Mirkin, C. A. *Chem. Rev.* **2005**, *105*, 1547−1562.
(10) Cao, Y. C.; Jin, R.; Mirkin, C. A. *Science* **2002**, *297* (5586), 1536−1540.
(11) Nicewarner-Peña, S. R.; Freeman, G.; Reiss, B. D.; He, L.; Peña, D. J.; Walton, I. D.; Cromer, R.; Keating, C. D.; Natan, M. J. *Science* **2001**, *294* (5540), 137−141.
(12) Tok, J. B.-H.; Chuang, F. Y. S.; Kao, M. C.; Rose, K. A.; Pannu, S. S.; Sha, M. Y.; Chakarova, G.; Penn, S. G.; Dougherty, G. M. *Angew. Chem., Int. Ed.* **2006**, *45*, 6900−6904.
(13) Stoermer, R. L.; Cederquist, K. B.; McFarland, S. K.; Sha, M. Y.; Penn, S. G.; Keating, C. D. *J. Am. Chem. Soc.* **2006**, *128*, 16892−16903.
(14) Eastman, P. S.; Ruan, W.; Doctolero, M.; Nuttall, R.; de Feo, G.; Park, J. S.; Chu, J. S. F.; Cooke, P.; Gray, J. W.; Li, S.; Chen, F. F. *Nano Lett.* **2006**, *6*, 1059−1064.
(15) Zanardi, P.; Rossi, F. *Phys. Rev. Lett.* **1998**, *81*, 4752−4755.
(16) Gunnarsson, L. *Appl. Phys. Lett.* **2001**, *78*, 802−804.
(17) Han, M.; Gao, X.; Su, J. Z.; Nie, S. *Nat. Biotechnol.* **2001**, *19*, 631−635.
(18) Qin, L.; Park, S.; Huang, L.; Mirkin, C. A. *Science* **2005**, *309*, 113−115.
(19) Qin, L.; Zou, S.; Xue, C.; Atkinson, A.; Schatz, G. C.; Mirkin, C. A. *Proc. Natl. Acad. Sci. U.S.A.* **2006**, *103* (36), 13300−13303.
(20) Orendorff, C. J.; Gole, A.; Sau, T. K.; Murphy, C. *J. Anal. Chem* **2005**, *77*, 3261−3266.
(21) Nie, S.; Emory, S. R. *Science* **1997**, *275* (5303), 1102−1106.
(22) Kneipp, K. *Phys. Rev. Lett.* **1997**, *78*, 1667−1670.
(23) Jeanmaire, D. L.; Van Duyne, R. P. *J. Electroanal. Chem* **1977**, *84*, 1−20.
(24) Martin, C. R. *Science* **1994**, *266*, 1961−1966.
(25) Possin, G. E. *Rev. Sci. Instrum.* **1970**, *41*, 772−774.
(26) Preston, C. K.; Moskovits, M. J. *J. Phys. Chem.* **1993**, *97*, 8495−8503.
(27) Wang, H.; Levin, C. S.; Halas, N. J. *J. Am. Chem. Soc.* **2005**, *127*, 14992.
(28) Fromm, D. P.; Sundaramurthy, A.; Schuck, P. J.; Kino, G.; Moerner, W. E. *Nano Lett.* **2004**, *4*, 957−961.
(29) Kim, J.; Liu, G. L.; Lee, L. P. *Opt. Express* **2005**, *13*, 4780−4785.

NL072606S